Eur. Phys. J. A **12**, 169–184 (2001)

THE EUROPEAN PHYSICAL JOURNAL A

Combinatorial nuclear level densities based on the Gogny nucleon-nucleon effective interaction

S. Hilaire[a], J.P. Delaroche, and M. Girod

Commissariat à l'Energie Atomique, Service de Physique Nucléaire, Boîte Postale 12, 91680 Bruyères-le-Châtel, France

Received: 13 February 2001 / Revised version: 17 September 2001
Communicated by P. Schuck

Abstract. A combinatorial method to calculate total level densities from an arbitrary single-particle level scheme is presented. Parity, angular momentum, pairing correlations as well as collective enhancements are explicitly treated. This method is employed using single-particle level schemes obtained from Hartree-Fock-Bogoliubov calculations based on the Gogny effective interaction. Sixty five even-even nuclei with masses $26 \leq A \leq 250$ are considered. Rather good agreements are obtained when comparing our predictions with experimental data for energies of the order of the neutron binding energies and for low excitation energies where discrete levels are experimentally observed.

PACS. 24.10.Pa Thermal and statistical models – 21.60.Jz Hartree-Fock and random-phase approximations – 21.10.Re Collective levels

1 Introduction

Calculations of cross-sections in the framework of statistical or pre-equilibrium models of nuclear reactions require the knowledge of various excited levels of the nucleus. From the analysis of the first discrete levels that can be experimentally observed, it is well known that their mean spacing decreases exponentially when the excitation energy increases. In other words, the total number of excited levels up to a given excitation energy U increases exponentially with U [1,2]. Therefore, above a few MeV of excitation energy, the number of excited levels is so large that it is impossible to track each of them individually. Consequently, the only tractable approach is statistical in nature and consists in considering a level density function.

Many theoretical and empirical studies have been conducted during the past sixty years to provide either analytical expressions or numerical evaluations for both particle-hole (p-h) or total level densities (LDs). Concerning p-h LDs, analytical expressions obtained within the equidistant spacing model [3–7] are generally employed even if more refined expressions accounting for shell or pairing effects [8–10] as well as more fundamental approaches [11–15] are available. The same remark hold for total LDs. Many theoretical approaches based on combinatorial technics [16–18], shell model Monte Carlo methods [19–21], spectral distribution calculations [22,23] or other realistic statistical methods [24–28] have been developed. However these rigorous methods are generally too complex to be used extensively in practical applications, and instead, rather simple [29–31] or more refined [32–35] analytical expressions depending on adjustable parameters are generally prefered. The main problem is that the amount of data available to optimize the key parameters is very limited. Therefore, extrapolating these parameters, as functions of energy or mass number for instance, is questionable, unless these extrapolations rely on theoretical approaches whose predictive power is well established.

One of the most powerful theory in nuclear-structure studies is the Hartree-Fock-Bogoliubov (HFB) mean-field method [36,37] implemented with the finite-range, density-dependent Gogny effective interaction (D1S) [38]. This mean-field method and its extensions have been successfully employed in various fields of nuclear structure [39–46], in particular for predicting collective levels at low excitation energies [47–49] and shape coexistence phenomena [50]. However, considering the number of excited levels that already exists for a few MeV of excitation energy (several millions for actinides at $U \approx 6$ MeV for instance), it is clear that a complete and rigorous microscopic calculation of each level is intractable within reasonable computational time. Therefore, one has to consider an alternative method, which, on the one hand, exploits the results from the HFB + D1S method, and, on the other hand, enables us to calculate LDs with good accuracy from low up to high excitation energies.

The goal of this article is to show that a combinatorial approach can fulfill these two conditions, provided that a few simplifying assumptions are made. For convenience, our present study is restricted to even-even nuclei

[a] e-mail: stephane.hilaire@cea.fr

all assumed with mirror axially symmetric shapes. Enforcing mirror axially symmetric shape enables us to define both the projection of the total spin of the nucleus on its symmetry axis, and its parity. Thus, calculating LDs as functions of excitation energy, spin and parity becomes feasible.

In sects. 2 and 3, we describe the models and methods we use to perform combinatorial level density calculations. We first generalize the combinatorial approach of ref. [7] to account for the spin projections and parities of the single-particle spectra. We then describe the way we include collective effects and pairing correlations, and finally derive level densities. Section 4 is devoted to the discussion of the ingredients needed to perform the actual LDs calculations. We briefly describe how the single-particle and single-hole states are obtained using the HFB + D1S method, and discuss the information (*i.e.*, vibrational states and moments of inertia) used to account for collective effects. Our predictions are finally compared in sect. 5 with experimental data on level densities for excitation energies close to the neutron binding energy B_n. We also show that our results reproduce reasonably well the energy dependence of the cumulated spectra built from discrete levels observed for excitation energies much lower than B_n.

2 Combinatorial method in the intrinsic frame

This section is devoted to the description of nuclear excitations in the intrinsic frame of coordinates. More precisely, we present the combinatorial method employed to calculate state densities (SDs)[1]. We first describe what we call particle-hole (p-h) state densities and also explain how these are calculated. We then consider the vibrational states which are here viewed and treated as a second category of intrinsic states.

2.1 Intrinsic particle-hole state densities

The starting point of our method is the formalism presented in ref. [7]. In this basic paper, it has been shown that, within the Independent Particle Model (IPM) framework, the values of the p-h SDs as a function of excitation energy can be deduced from the grand partition function $\mathcal{Z}$ expressed in terms of the energies of the single-particle–single-hole states of a nucleus. In order to calculate SDs as functions of excitation energy, spin projections and parity, we have generalized the aforementioned combinatorial method as is now described.

2.1.1 Basic definitions

We must first point out, that a clear-cut distinction between particles and holes is possible only if pairing correlations are neglected. In a first step, we therefore ignore such correlations. These will be included later on (subsect. 3.2) in an approximate manner to produce our final predictions.

A mirror axially symmetric nucleus may be represented by two sets of single-particle states (one for the protons and the other for the neutrons). Each individual state is characterized by its energy ε, angular-momentum projection m (*i.e.*, projection of the spin on the intrinsic symmetry axis of the nucleus) and parity p. Following closely the notations adopted in ref. [7], we first define the single-particle–single-hole states as

$$\left.\begin{array}{l} \varepsilon_i^1 = \varepsilon_{F_\pi+i}^\pi - \varepsilon_{F_\pi}^\pi \\ m_i^1 = m_{F_\pi+i}^\pi \\ p_i^1 = p_{F_\pi+i}^\pi \end{array}\right\}, \quad i = 1, ..., I_1\,, \tag{1}$$

$$\left.\begin{array}{l} \varepsilon_i^2 = \varepsilon_{F_\pi}^\pi - \varepsilon_{F_\pi-i+1}^\pi \\ m_i^2 = -m_{F_\pi-i+1}^\pi \\ p_i^2 = p_{F_\pi-i+1}^\pi \end{array}\right\}, \quad i = 1, ..., I_2\,, \tag{2}$$

$$\left.\begin{array}{l} \varepsilon_i^3 = \varepsilon_{F_\nu+i}^\nu - \varepsilon_{F_\nu}^\nu \\ m_i^3 = m_{F_\nu+i}^\nu \\ p_i^3 = p_{F_\nu+i}^\nu \end{array}\right\}, \quad i = 1, ..., I_3\,, \tag{3}$$

$$\left.\begin{array}{l} \varepsilon_i^4 = \varepsilon_{F_\nu}^\nu - \varepsilon_{F_\nu-i+1}^\nu \\ m_i^4 = -m_{F_\nu-i+1}^\nu \\ p_i^4 = p_{F_\nu-i+1}^\nu \end{array}\right\}, \quad i = 1, ..., I_4\,, \tag{4}$$

for proton particles, proton holes, neutron particles and neutron holes, respectively.

In eqs. (1)-(4), F_π (respectively F_ν) is an index for the last occupied proton (respectively neutron) state in the ground state of a nucleus. The minus signs appearing in the definition of the holes' spin projections enable us to take into account the fact that when a particle-hole excitation is considered, the contribution of the hole to the total-spin projection M of the nucleus is opposite to that of the state on which the hole has been created. Finally, the indexes I_1,..., I_4 denote the number of discrete states considered for each sets of single-particle–single-hole states. In pratice, $I_2 = Z$ and $I_4 = N$ for a nucleus with Z protons and N neutrons while I_1 and I_3 are restricted by the maximum excitation energy up to which one is interested. However, we keep the I_k indexes in the equations for convenience.

We then consider a nuclear excited state built from independent particle-hole excitations. A state with N_1 proton particles, N_2 proton holes, N_3 neutron particles and N_4 neutron holes is labeled as $\mathcal{N} = (N_1, N_2, N_3, N_4)$. Using the notations introduced in eqs. (1)-(4), the state density $\rho_{\mathcal{N}}(U, M, P)$ for a given configuration $\mathcal{N}$, a given excitation energy U, a given spin projection M and a given parity P is the number of solutions per unit energy of the set of equations

$$U = \sum_{k=1}^{4} \sum_{i=1}^{I_k} n_i^k\, \varepsilon_i^k\,, \tag{5}$$

[1] The only difference between SDs and LDs is that the state densities depend on the projections of spins on the symmetry axis in the intrinsic frame of the nucleus, whereas level densities are expressed in terms of the nucleus spin J, in the laboratory frame.

$$M = \sum_{k=1}^{4} \sum_{i=1}^{I_k} n_i^k \, m_i^k, \tag{6}$$

$$P = \prod_{k=1}^{4} \prod_{i=1}^{I_k} (p_i^k)^{n_i^k}, \tag{7}$$

$$N_k = \sum_{i=1}^{I_k} n_i^k \ , \qquad k = 1, 2, 3, \text{ or } 4, \tag{8}$$

where $n_i^k = 0$ or 1 if the state i is empty or occupied, respectively.

2.1.2 Combinatorial formalism

To formally determine the total number of solutions of eqs. (5)-(8), we define the generating function $\mathcal{Z}$:

$$\mathcal{Z}(x_1, x_2, x_3, x_4, y, t) = \prod_{k=1}^{4} \prod_{i=1}^{I_k} \left(1 + x_k \, p_i^k \, y^{\varepsilon_i^k} \, t^{m_i^k}\right). \tag{9}$$

This generating function is a straightforward generalization of that used previously in ref. [7] to account not only for energy but also for spin projection and parity. Indeed, the variables x_k, $(k = 1, ..., 4)$ enable us to count the number of particles and holes, y enables us to keep track of the excitation energies and t of the spin projections. $\mathcal{Z}$ can be expanded in powers of x_k writing

$$\mathcal{Z}(x_1, x_2, x_3, x_4, y, t) = \sum_{\mathcal{N}} \mathcal{F}_{\mathcal{N}}(y, t) \prod_{k=1}^{4} x_k^{N_k} \ , \tag{10}$$

the symbol $\mathcal{N}$ denoting again any integers combination (N_1, N_2, N_3, N_4). If we furthermore expand the function $\mathcal{F}_{\mathcal{N}}(y, t)$ into powers of y and t writing

$$\mathcal{F}_{\mathcal{N}}(y, t) = \sum_{U} \sum_{M} \sum_{P=-1,+1} C_{\mathcal{N}}(U, M, P) \; y^U \, t^M, \tag{11}$$

it is then trivial that the coefficients $C_{\mathcal{N}}(U, M, P)$ are exactly the numbers of solutions of eqs. (5)-(8) we are seeking for. To calculate the $C_{\mathcal{N}}$ coefficients, we use the mathematical tools of ref. [7] and write $\mathcal{F}_{\mathcal{N}}(y, t)$ as

$$\mathcal{F}_{\mathcal{N}}(y, t) = \prod_{k=1}^{4} \sum_{\{\alpha(N_k)\}} \prod_{j=1}^{N_k} \frac{1}{\alpha_j^k!} \times \left[\sum_{i=1}^{I_k} \frac{(-1)^{j+1}}{j} (p_i^k)^j \; y^{j\varepsilon_i^k} \; t^{j m_i^k}\right]^{\alpha_j^k}, \tag{12}$$

where the symbol $\{\alpha(N_k)\}$ means all the integers combinations $(\alpha_1^k, \alpha_2^k, ..., \alpha_{N_k}^k)$ that satisfy the relation

$$\alpha_1^k + 2\,\alpha_2^k + ... + N_k \, \alpha_{N_k}^k = N_k. \tag{13}$$

Following the ensemble theory terminology, we call such combinations the partitions of N_k.

As can be seen in table 1, the number $D(N_k)$ of such partitions increases very rapidly with increasing N_k values. Therefore, to save computing time, these partitions are calculated once for all.

Table 1. Number $D(N_k)$ of partitions of N_k.

N_k	1	7	13	20	27	34	41
$D(N_k)$	1	15	101	627	3010	12310	44583

2.1.3 Numerical method

The next step consists in calculating the coefficients $C_{\mathcal{N}}$ simultaneously for all the excitation energies of interest. For this purpose, the single-particle energies ε_i^k are first expressed in terms of an energetic arbitrary unit ε_0, writing

$$\varepsilon_i^k = \nu_i^k \ \varepsilon_0 \ , \tag{14}$$

with ν_i^k as an integer. This transformation enables us to represent each sum

$$S_j^k = \sum_{i=1}^{I_k} \frac{(-1)^{j+1}}{j} \; (p_i^k)^j \; y^{j\varepsilon_i^k} \; t^{j m_i^k}$$

appearing in eq. (12) by the element $M_{S_j^k}(n, m, p)$ of the matrix $\mathcal{M}_{S_j^k}$, such that

$$M_{S_j^k}(n, m, p) = \sum_{i=1}^{I_k} \frac{(-1)^{j+1}}{j} \delta(n - j\nu_i^k) \times \delta(m - 2j m_i^k) \delta(p - p_{i,k}^j) \, . \tag{15}$$

In eq. (15), the factor 2 attached to the term $j \, m_i^k$ makes it possible to overcome the problem of half-integer values taken by the spin projections m_i^k. Moreover, $p_{i,k}^j$ is defined by $p_{i,k}^j = 1$ (respectively 0) if $(p_i^k)^j = -1$ (respectively $+1$), and $\delta(x) = 1$ if $x = 0$ and 0 otherwise.

With such definitions and notations, we then define i) the matrix $\mathcal{M}_{P+Q}$, sum of $\mathcal{M}_P$ and $\mathcal{M}_Q$, by

$$M_{P+Q}(n, m, p) = M_P(n, m, p) + M_Q(n, m, p) \ ,$$

and ii) the matrix $\mathcal{M}_{PQ}$, product of $\mathcal{M}_P$ and $\mathcal{M}_Q$, by

$$M_{PQ}(n, m, p) = \sum_{i+j=n} \sum_{k+l=m} M_P(i, k, 0) \; M_Q(j, l, 0) + M_P(i, k, 1) \; M_Q(j, l, 1),$$

for positive parity $(p = 0)$ and by

$$M_{PQ}(n, m, p) = \sum_{i+j=n} \sum_{k+l=m} M_P(i, k, 0) \; M_Q(j, l, 1) + M_P(i, k, 1) \; M_Q(j, l, 0),$$

for negative parity $(p = 1)$.

Using these techniques, the matrix $\mathcal{M}_{\mathcal{F}_{\mathcal{N}}}$ representing the function $\mathcal{F}_{\mathcal{N}}$ in eqs. (11) and (12), reads

$$\mathcal{M}_{\mathcal{F}_{\mathcal{N}}} = \prod_{k=1}^{4} \sum_{\{\alpha(N_k)\}} \prod_{j=1}^{N_k} \frac{1}{\alpha_j^k!} \left[\mathcal{M}_{S_j^k}\right]^{\alpha_j^k}.$$

Finally, the coefficients $C_{\mathcal{N}}$ are obtained as

$$C_{\mathcal{N}}(U,M,P) = M_{\mathcal{F}_{\mathcal{N}}}(n,m,p), \tag{16}$$

where $m = 2\,M$, $p = 0$ (respectively 1) if $P = +1$ (respectively -1) and where the integer n is deduced from the relation

$$\left(n - \frac{1}{2}\right)\varepsilon_0 \leq U < \left(n + \frac{1}{2}\right)\varepsilon_0.$$

Therefore, the $C_{\mathcal{N}}(U,M,P)$ coefficients we calculate are not exactly the numbers of solutions of eqs. (5)-(8), but rather the numbers of solutions of eqs. (5)-(8) in an energy interval of width ε_0 centered around the excitation energy U.

2.1.4 From the $C_{\mathcal{N}}(U,M,P)$ coefficient to the particle-hole state density $\rho_{\mathcal{N}}(U,M,P)$

The final step consists in deriving the p-h SDs, $\rho_{\mathcal{N}}$, from the $C_{\mathcal{N}}$ coefficients obtained from eq. (16). The simplest definition for $\rho_{\mathcal{N}}$ reads

$$\rho_{\mathcal{N}}(U,M,P) = \frac{1}{\varepsilon_0}\; C_{\mathcal{N}}(U,M,P). \tag{17}$$

However, the problem with eq. (17) is that the state densities $\rho_{\mathcal{N}}$ turn out to be strongly dependent on ε_0. Using too weak an ε_0-value does not lead to smooth state densities as functions of excitation energy. We therefore employ another method suggested by Williams [16] to limit the discretization effects as explained below.

Summing all the $C_{\mathcal{N}}$-values up to a given excitation energy U, we first obtain the cumulated number of states $N_{\mathcal{N}}(U,M,P)$ which represents the number of p-h states with excitation energy E such that $0 \leq E \leq U$. The p-h state density defined as

$$\rho_{\mathcal{N}}(U,M,P) = \frac{\mathrm{d}N_{\mathcal{N}}(U,M,P)}{\mathrm{d}U}\,,$$

can also be written as

$$\rho_{\mathcal{N}}(U,M,P) = \; N_{\mathcal{N}}(U,M,P)\; \frac{\mathrm{d}\ln N_{\mathcal{N}}(U,M,P)}{\mathrm{d}U}\,. \tag{18}$$

In eq. (18), $\mathrm{d}\ln N_{\mathcal{N}}(U,M,P)/\mathrm{d}U$ and $N_{\mathcal{N}}(U,M,P)$ are deduced from a linear interpolation, over an energy interval of width δU centered on U, of the combinatorial $\ln N_{\mathcal{N}}(U,M,P)$-values. We have checked that the results obtained in this manner, were not too much sensitive to the width δU nor to the ε_0-value. Except for specific nuclei that will be discussed later on, an interval of width $\delta U = 0.2$ MeV is used to determine $\rho_{\mathcal{N}}(U,M,P)$. Concerning ε_0, we have performed several calculations with $\varepsilon_0 = 0.5, 0.1, 0.05, 0.01$ and 0.001 MeV and we have found that the value $\varepsilon_0 = 10$ keV was the best compromise to get a reasonable calculation time together with the stability of the calculated level densities. Indeed, for ε_0-values lower than 10 keV, the calculated level densities remain unchanged, while one observes differences for higher ε_0-values. Therefore $\varepsilon_0 = 10$ keV has been systematically adopted (see subsubsect. 5.1.1).

Once these particle-hole intrinsic $\rho_{\mathcal{N}}$-values are determined, the intrinsic state density ρ_{int} is then simply obtained by summing the $\rho_{\mathcal{N}}$-values for which $N_1 = N_2$ and $N_3 = N_4$.

2.2 Intrinsic vibrational state densities

Until now, we have only considered independent (incoherent) particle-hole excitations. Nevertheless, nuclei also display collective excitations which may be viewed as superpositions of coherent p-h excitations. These collective modes fall into two categories, rotations and vibrations, which in actual nuclei are often coupled modes. In the present work, both types of collective excitations are considered and treated in the adiabatic approximation. More precisely, we deliberately ignore the underlying p-h structure of these collective modes and assume that i) the excitation energy in a nucleus involves both non-collective and collective degrees of freedom, and ii) there exists no interaction between collective and p-h states as well as between vibration and rotation modes. Since spherical and deformed nuclei can vibrate, we treat vibrational states in the intrinsic frame of coordinates as explained below.

We still consider an axially mirror symmetric nucleus, and use the fact that the vibrational (phonon) states of a nucleus obey the Bose-Einstein statistics to describe them with the generalized boson generating function

$$\mathcal{Z}_{\mathrm{vib}}(x,y,t) = \prod_{\lambda}\prod_{\mu}\sum_{N=0}^{+\infty}\left[x\; y^{\varepsilon_{\lambda\mu}}\; t^{\mu}\; p_{\lambda}\right]^{N}, \tag{19}$$

where x, y and t enable us to keep track of the number of bosons as well as of their excitation energies and spin projections. In this equation, $\varepsilon_{\lambda\mu}$ is the energy of a phonon with multipolarity λ and spin projection μ ($-\lambda \leq \mu \leq \lambda$). Furthermore, $p_{\lambda} = (-1)^{\lambda}$ and $p_{\lambda} = (-1)^{\lambda+1}$ for isoscalar and isovector phonons, respectively.

For spherical nuclei, the energies $\varepsilon_{\lambda\mu}$ are $(2\lambda+1)$-fold degenerate for a phonon of multipolarity λ and μ takes on all the integer values between $-\lambda$ and $+\lambda$. In contrast, for deformed nuclei, the $\varepsilon_{\lambda\mu}$-values are no longer degenerate. Also, some μ-values are ruled out for quadrupole modes as a result of symmetries imposed to nuclear shapes and collective wave functions [51]. Indeed, only the projections $\mu = 0$ (β vibrations) and ± 2 (γ vibrations) survive for the $\lambda = 2$ mode. Therefore, for quadrupole phonons in deformed nuclei, the product over μ in eq. (19) is restricted to $\mu = -2$, 0 and 2. For other multipoles modes, all possible μ-values are kept since the symmetries imposed to nuclear shapes and collective wave functions are already taken into account for quadrupole modes.

Thanks to the matrix method described in subsect. 2.1, it is then trivial to calculate the matrix $\mathcal{M}_{\mathrm{vib}}$ representing the partition function $\mathcal{Z}_{\mathrm{vib}}$ of eq. (19). Furthermore, one can easily consider a restricted number N of phonons by

truncating the expansion (19) up to the order x^N. This truncation is an *ad hoc* mean of accounting for the loss of collectivity observed in nuclei when the number of coupled phonons gradually increases. In other words, multiphonon states with $N \geq 3$ are weakly collective in nature and usually interpreted in terms of simple admixtures of uncorrelated p-h excitations. An obvious advantage of such a truncation thus lies in avoiding double counting. Of course, one can form any coupling between the various multipoles considered in the calculation, as it has been experimentally evidenced [52–63], but the total number of coupled phonons $N_{\rm tot}$ will never exceed 3 in our approach.

In summary, we have described the way we compute separately the two intrinsic (*i.e.*, particle-hole and vibrational) state densities. However, even if we assume that the vibrational and the particle-hole excitations are independent phenomena, a given particle-hole excitation can also "vibrate" [64]. In other words, we have to fold in the vibrational ($\rho_{\rm vib}$) and the intrinsic p-h ($\rho_{\rm int}$) state densities to deduce the total intrinsic state density $\rho_{i*v}(U, M, P)$.

3 Level densities in the laboratory frame

This section describes the ways the level densities are built from the total intrinsic state density ρ_{i*v}. We first explain how the rotational motion is included. We then describe various approximations to deal with pairing correlations.

3.1 Restoration of rotational invariance

The level densities are obtained following two methods tailored to treat separately spherical and deformed nuclei.

3.1.1 Spherical nuclei

If the nucleus under consideration displays spherical symmetry, the intrinsic and laboratory frames coincide, and the level density is trivially obtained through the relation

$$\rho(U, J, P) = \rho_{i*v}(U, M = J, P) - \rho_{i*v}(U, M = J+1, P). \quad (20)$$

3.1.2 Deformed nuclei

For deformed nuclei, rotational motion has to be explicitly treated. For an axially mirror symmetric nucleus, rotation takes place around an axis perpendicular to the nucleus symmetry axis. In this case, any intrinsic state of specified spin projection K and parity P is the band head of a set of levels having the same parity P and spins $J = K, K+1, K+2, ...$ if $K \neq 0$, and $J = 0, 2, 4, ...$ or $1, 3, 5, ...$ if $K^P = 0^+$ or 0^-, respectively [65]. These sequences of levels form rotational bands in which each member's energy can be deduced from the band head energy, provided the difference $E_{\rm rot}^{J,K}$ between the energy of the level J^P and that of the band head state K^P is known. The level density for deformed nuclei then reads

$$\begin{aligned}\rho(U, J, P) = \frac{1}{2} \sum_{K=-J, K\neq 0}^{J} & \rho_{i*v}(U - E_{\rm rot}^{J,K}, K, P) \\ & + \delta_{(J\ \text{even})}\, \delta_{(P=+)}\, \rho_{i*v}(U - E_{\rm rot}^{J,0}, 0, P) \\ & + \delta_{(J\ \text{odd})}\, \delta_{(P=-)}\, \rho_{i*v}(U - E_{\rm rot}^{J,0}, 0, P)\,. \quad (21)\end{aligned}$$

In the first right-hand side term of eq. (21), the factor $1/2$ accounts for the fact that in mirror axially symmetric nuclei, the intrinsic states with spin projections $+K$ or $-K$ give rise to the same rotational levels. Moreover, in the second and third terms of the summation, the symbol $\delta_{(x)}$ (defined by $\delta_{(x)} = 1$, if x holds true, and 0 otherwise) restricts the rotational bands built on intrinsic states with spin projection $K = 0$ and parity P to the levels sequences $0, 2, 4, ...$ for $P = +$ and $1, 3, 5, ...$ for $P = -$.

We have previously labeled the intrinsic band head state densities on which the rotational bands are constructed as ρ_{i*v} (*i.e.*, the density obtained from folding in $\rho_{\rm int}$ and $\rho_{\rm vib}$), but one may, of course, neglect the vibrational states and thus use simply $\rho_{\rm int}$ to construct rotational bands. In this last case, we can already guess that ignoring vibrational states will imply an underestimate of the predicted LDs. It is however interesting to study both situations in order to estimate the importance of including the vibrational states in our level density predictions. Whatever the choice made, pairing effects must also be taken into account. We thus now focus on the possible methods that we consider to approximate these latter effects.

3.2 Pairing correlations

In this section, we only consider intrinsic particle-hole state densities. It is well known that in order to create a particle-hole excitation, it is generally necessary to bring in more energy than the simple difference between the energy of the last occupied single-particle state and that of the first empty one. This extra energy is called pairing energy and corresponds to the fact that a pair of nucleons must be broken before exciting one of its components. Here, we discuss several ways of including pairing correlations in our model and suggest which one seems to be the best.

The most often used approximation to deal with pairing correlations consists in assuming that once a pair has been broken, the nucleus behaves like in the Independent Particle Model (IPM). Under such an assumption the paired state density $\rho_{\mathcal{N}}^{\rm paired}$ (*i.e.*, including pairing effects) is deduced from that calculated within the IPM framework ($\rho_{\mathcal{N}}^{\rm unpaired}$, calculated as in subsubsect. 2.1.4) by simply introducing a shift in the excitation energy, such that

$$\rho^{\rm paired}(U) = \rho^{\rm unpaired}(U - \Delta)\ , \quad (22)$$

with $\Delta = 0$, δ or 2δ for odd-odd, odd, or even-even nuclei, respectively. In this approximation, the empirical energy δ

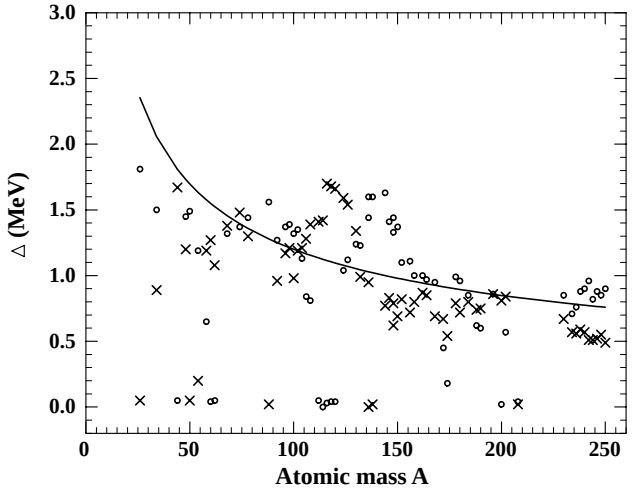

Fig. 1. Comparison between the empirical pairing energy $\delta = 12/\sqrt{A}$ (full line) and the HFB + D1S calculated Δ_n (crosses) and Δ_p (circles) values.

is generally assumed to be the systematic odd-even mass difference in nuclei (*i.e.*, $\delta \approx 12/\sqrt{A}$ MeV). However, using such a shift will certainly lead to underestimating the state densities for the following reasons:

i) First, particle-hole configurations which only involve one kind of fermion should only be shifted by δ, even for an even-even nucleus. In other words, a shift $\Delta = 2\delta$ only holds for particle-hole configurations involving both neutrons and protons.
ii) Second, there might be significant differences between the neutron and proton pairing energies. In particular, the pairing energy in nuclei is known to be very weak near shell closure.
iii) Third, the only states for which pairing effect is significant are those which are close to the last occupied state (Fermi level) in the ground state of a nucleus. Therefore, particle-hole excitations involving states far enough from the Fermi level should not be treated with the empirical shift mentioned above.
iv) Finally, eq. (22) implies that odd-odd nuclei are not affected by pairing correlations, which turns out to be a wrong statement if other single-particle states than the odd one are excited. However, since our present study is restricted to even-even nuclei, we will not consider this last point.

A simple solution to these problems is obtained by solving the HFB equations assuming that the off-diagonal terms of the pairing field are small. This is a good approximation to the HFB solutions [39], which provides single-particle and single-hole states with energies ε_i^k, spin projection m_i^k, and parity p_i^k (see eqs. (1)-(4)), as well as pairing energies Δ_i^k. Using these pairing energies, we can then consider two different approximations to account for pairing effects in LDs:

i) The simplest method consists in using the microscopic counterparts of the empirical energy correction δ, defined as

$$\Delta_p = \Delta_1^2\,, \quad \text{for protons} \tag{23}$$

and

$$\Delta_n = \Delta_1^4\,, \quad \text{for neutrons,} \tag{24}$$

which both represent microscopic values of the differences between the energy of first p-h excitation when pairing correlations are accounted for and ignored. As can be seen in fig. 1, the HFB + D1S Δ_n and Δ_p-values, shown as crosses and circles, respectively, behave roughly like the empirical pairing shift $\delta = 12/\sqrt{A}$, but important deviations are found, especially for nuclei with numbers of protons and/or neutrons close to magic numbers. As mentioned previously, Δ_n and/or Δ_p are found to be negligible for such nuclei. Therefore, this first approach enables us to replace the systematic pairing shift when it is known to be too strong. However, it cannot account for the different shift that should be applied to particle-hole excitations involving single-particle states close to, or far from the Fermi level.

ii) The second method enables us to study the aforementioned problem, as we now explain. We calculate the cumulated number of states $N_{\mathcal{N}}(E)$ given by

$$N_{\mathcal{N}}(E) = \sum_M \sum_P N_{\mathcal{N}}(E, M, P)\,,$$

where $N_{\mathcal{N}}(E, M, P)$ is defined in subsubsect. 2.1.4, for the three configurations $\mathcal{N} = (1, 1, 0, 0)$, $\mathcal{N} = (0, 0, 1, 1)$ as well as $\mathcal{N} = (1, 1, 1, 1)$, with and without accounting for pairing correlations. Pairing correlations are treated explicitly by changing the holes states energies ε_i^k ($k = 2$ for protons and 4 for neutrons) into $\sqrt{(\varepsilon_i^k)^2 + (\Delta_i^k)^2}$. One can then easily deduce (see fig. 2(a) for the $\mathcal{N} = (1, 1, 0, 0)$ configuration) the pairing shift $\Delta_{\mathcal{N}}(U)$ between the unpaired cumulated number of states $N_{\mathcal{N}}^{\text{unpaired}}$ and the paired one $N_{\mathcal{N}}^{\text{paired}}$ as a function of the excitation energy U. Three energy-dependent shifts (*i.e.*, $\Delta_p(U)$ for the proton configuration $\mathcal{N} = (1, 1, 0, 0)$, $\Delta_n(U)$ for the neutron configuration $\mathcal{N} = (0, 0, 1, 1)$ and $\Delta_{p+n}(U)$ for the proton-neutron configuration $\mathcal{N} = (1, 1, 1, 1)$) are thus calculated. These shifts are then used for all the particle-hole configurations considered in the calculations, following the aforementioned assumption that once a pair has been broken, the nucleus behaves like in the IPM. In other words, the pairing shift used to account for pairing correlations in any configuration $\mathcal{N} = (N_\pi, N_\pi, N_\nu, N_\nu)$ is $\Delta_p(U)$, if $N_\nu = 0$ and $N_\pi \neq 0$, $\Delta_n(U)$, if $N_\pi = 0$ and $N_\nu \neq 0$ and $\Delta_{p+n}(U)$, if both $N_\nu \neq 0$ and $N_\pi \neq 0$. For instance, let us consider the proton particle-hole configuration $\mathcal{N} = (3, 3, 0, 0)$. The associated unpaired number of cumulated states $N_{\mathcal{N}}^{\text{unpaired}}$ vanishes below a given threshold $U_{\mathcal{N}}$. To account for the pairing effect at a given excitation energy U, we apply the procedure illustrated by fig. 2(b), and write

$$N_{\mathcal{N}}^{\text{paired}}(U) = N_{\mathcal{N}}^{\text{unpaired}}(U - \Delta_p(U - U_{\mathcal{N}})). \tag{25}$$

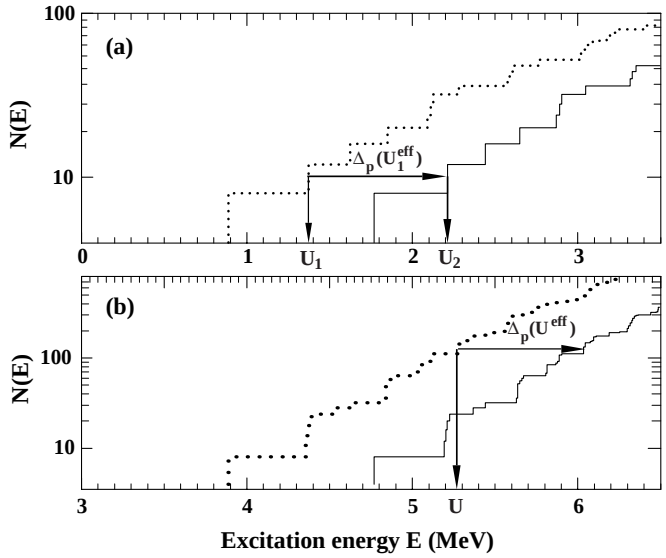

Fig. 2. Comparison between the calculated number of levels up to an excitation energy E with (full line) and without (dotted line) pairing as a function of the excitation energy E. (a) The proton configuration $\mathcal{N} = (1,1,0,0)$ for ^{238}U is considered. The shift $\Delta_p(U_1^{\rm eff})$ is the energy difference $U_2 - U_1$, where U_1 and U_2 are such that $N_{\mathcal{N}}^{\rm unpaired}(U_1) = N_{\mathcal{N}}^{\rm paired}(U_2)$. The effective excitation energy is given by $U_1^{\rm eff} = U_1 - U_{(1,1,0,0)}$, where $U_{(1,1,0,0)}$ is the threshold below which $\mathcal{N}_{(1,1,0,0)} = 0$. (b) The way $N_{(3,3,0,0)}^{\rm paired}$ is deduced from $N_{(3,3,0,0)}^{\rm unpaired}$ for ^{238}U is shown. In this case $U^{\rm eff} = U - U_{(3,3,0,0)}$.

Finally, the state density $\rho_{\mathcal{N}}^{\rm paired}$ is deduced from the calculated $N_{\mathcal{N}}^{\rm paired}$-values following the method described previously in subsubsect. 2.1.4.

4 Ingredients for actual calculations

In this section we discuss the main features of the nuclei under study and inputs to our calculations. We first explain how the HFB + D1S single-particle levels are obtained and then describe the way the vibrational states are accounted for. Finally, we discuss the method used to account as well for the rotational motion of deformed nuclei.

4.1 HFB + D1S intrinsic single-particle states

As indicated in sect. 1, we only consider the 65 even-even nuclei for which experimental data at B_n are given in ref. [66]. The HFB + D1S method is used to determine the single-particle level schemes used in eqs. (1)-(4) to define particle and hole states. All the nuclei considered in our study are described using the unconstrained HFB + D1S method which consists in minimizing the nuclear ground-state energies with respect to the axial deformation parameter β defined as

$$\beta = \sqrt{\frac{\pi}{5}} \frac{\langle Q_{20}^M \rangle}{AR^2} \,,$$

where $\langle Q_{20}^M \rangle$ is the mass quadrupole moment, and where $R^2 = 3/5 r_0^2 A^{2/3}$ with $r_0 = 1.2$ fm.

The proton and neutron single-particle level schemes used in our combinatorial approach are obtained for the deformations β_0 which yield the lowest HFB energies. As mentioned previously, the BCS-like approximation discussed in ref. [39] is used only to obtain single-particle energies as well as single-particle pairing energies.

4.2 Vibrational states

To compute the vibrational intrinsic level densities, it is necessary to know the energies of the phonon states entering eq. (19). For this purpose, we use the experimental values taken from ref. [67] and shown in table 2.

As pointed out in subsect. 2.2, λ-multipole phonons in spherical nuclei are $(2\lambda+1)$-fold degenerate. Therefore, to form only one set of experimental data for both spherical and deformed nuclei under consideration, we have put in column "β" the quadrupole phonon energy and left empty column "γ" for spherical nuclei.

The way these data are used to calculate ρ_{i*v} depends upon whether the nucleus is spherical or deformed:

i) For spherical nuclei, we assume that the first 2^+ and 3^- excited levels are associated with the quadrupole and octupole mode energies, respectively. Because of spherical symmetry, each mode with multipolarity λ is $(2\lambda+1)$-fold degenerate.

ii) For deformed nuclei, two kinds of quadrupole vibration are observed, namely β and γ vibrations. The quadrupole mode energies are chosen as the first 0^+ excited level energy for the β vibration, and the first 2^+ (belonging neither to the β vibrational nor to the ground-state bands) for the γ vibration. Concerning the octupole modes, the problem is more complicated. Indeed, for light nuclei, only the $(\lambda,\mu) = (3,\pm 3)$ modes are experimentally observed. In contrast, for nuclei with masses $A > 150$, the levels associated with the $(\lambda,\mu) = (3,\pm 2)$, $(3,\pm 1)$ and $(3,0)$ modes are rather well established, while those associated with the $(\lambda,\mu) = (3,\pm 3)$ mode are not unambiguously identified. For instance, in ref. [68], the octupole $(\lambda,\mu) = (3,\pm 3)$ level is predicted above 6 MeV of excitation energy in the rare-earth mass region, whereas in ref. [69] it is assumed to have an excitation energy between 1 and 2.5 MeV. Because of this ambiguity, we have included, in table 2, the $(\lambda,\mu) = (3,\pm 3)$ modes with the energies found in refs. [67,69]. Indeed, if we assume that these modes are located above 6 MeV, it will certainly not influence our level density calculations up to B_n and it is therefore not necessary to include the $(\lambda,\mu) = (3,\pm 3)$ terms in eq. (19). In contrast, if we assume these modes at excitation energies below 2.5 MeV, we will use, in eq. (19), the excitation energies of table 2. Another ambiguity has been mentioned concerning the fact that, in the transitional region from spherical to well-deformed nuclei (^{146,148}Nd and ^{148}Sm), the assumed $K^P = 1^-$ octupole band

Table 2. Phonon energies in MeV. Brackets are added when band head levels energy or collective character is uncertain.

Z	N	$\lambda=2$		$\lambda=3$			
		β	γ	0	1	2	3
12	14	3.59	2.94				6.88
16	18	3.92	3.30				4.62
20	24	1.16					3.31
22	26	3.00	2.42				3.36
22	28	1.55					4.15
24	30	2.83	2.62				4.13
26	30	2.94	2.65				4.51
28	32	2.29	2.16				4.04
28	34	2.05	2.30				3.76
30	38	1.66	1.88				2.75
32	42	1.48	1.20				2.54
34	44	1.50	1.31				2.51
38	50	1.84					2.73
40	52	0.93					2.34
42	54	0.78					2.23
42	56	0.74	1.43				2.02
44	56	1.13	1.36				2.17
44	58	0.94	1.10				2.04
44	60	0.99	0.89				1.97
46	60	1.13	1.13				2.08
46	62	1.05	0.93				2.05
46	64	0.95	0.81				2.04
48	64	1.22	1.31				2.01
48	66	1.13	1.21				1.96
50	66	1.29					2.27
50	68	1.23					2.33
50	70	1.17					2.40
52	72	1.66	1.33				2.29
52	74	1.87	1.42				2.39
54	76	1.79	1.12				2.40
54	78	[1.8]	1.30				2.47
54	82	1.31					3.28
56	80	0.82					2.53
56	82	1.44					2.88
60	84	0.70					1.51
60	86	0.92	1.47		[1.3]		1.19
60	88	0.92	1.25		[1.0]		1.00
62	86	[1.4]	[1.4]		[1.4]		1.16
62	88	0.74	1.05		1.16	[1.7]	1.07
62	90	0.69	1.09	[0.9]	[1.5]	[1.6]	[2.0]
64	92	1.05	1.15	[1.3]	1.24	1.78	[1.9]
64	94	1.20	1.19	[1.2]	0.98	1.79	[1.7]
66	96	1.40	0.89	[1.2]	1.64	1.15	1.57
66	98	1.66	0.76	[1.6]	1.64	0.98	[1.7]
68	100	1.22	0.82	[1.7]	1.36	1.57	1.54
70	102	1.04	1.47	1.58	1.16	1.76	[2.0]
70	104	1.49	1.63	1.70	[1.2]	1.32	1.85
72	106	1.20	1.18	[1.7]	1.31	1.26	[1.8]
72	108	1.10	1.30	[2.0]	[1.4]	[1.3]	[1.3]
74	110	1.00	0.90	[1.7]	[1.6]	1.13	1.81
76	112	1.09	0.63	[1.7]	[1.5]	[1.4]	1.41
76	114	0.91	0.56	[1.9]	[1.8]	[1.6]	1.39
78	118	1.14	0.69				1.45
80	120	1.03	1.57				2.61
80	122	1.56	0.96				2.71
82	126	4.09					2.62
90	140	0.64	0.78	0.50	0.95	1.08	[1.5]
92	142	0.81	0.93	0.77	[0.9]	0.99	[1.3]
92	144	0.92	0.96	0.68	[0.9]	1.11	[1.1]
92	146	0.99	1.06	0.67	[0.9]	[1.1]	[1.4]
94	146	0.86	1.14	0.59	0.94	1.24	[1.2]
94	148	0.96	1.10	0.77	[1.0]	[1.1]	[1.2]
96	148	0.99	1.08	[1.1]	[1.0]	[0.7]	[1.2]
96	150	1.17	1.00	[1.2]	[1.0]	[0.7]	[1.3]
96	152	1.08	1.00	[1.2]	[1.1]	[0.7]	[1.3]
98	152	1.15	1.00	[1.3]	[1.1]	[0.9]	[1.2]

head state (see table 2) is uncertain and can instead be interpreted as stemming from the coupling between one-quadrupole and one-octupole phonons [57–59]. Our goal here is certainly not to discuss such ambiguities. We will therefore simply include, in eq. (19), the octupole modes using the excitation energies of table 2.

4.3 Rotational bands and moments of inertia

The last important ingredients needed for our calculations are the moments of inertia. We have seen in subsect. 3.1 that the only value needed in our model was the rotational energy $E_{\rm rot}^{J,K}$. Following the usually employed analytical formulae relevant to axially symmetric nuclei for $E_{\rm rot}^{J,K}$ [35], we write

$$E_{\rm rot}^{J,K} = \frac{J(J+1)-K^2}{2\mathcal{J}_\perp}. \tag{26}$$

In this equation, $\mathcal{J}_\perp$ is the moment of inertia of a nucleus rotating around an axis perpendicular to the symmetry axis. This moment of inertia is calculated in the Inglis-Belyaev approximation [70,71] from the HFB + D1S self-consistent mean-field solutions and renormalized as indicated in [45]. It is from now on labeled as $\mathcal{J}_\perp^{\rm D1S}$. The value taken by $\mathcal{J}_\perp^{\rm D1S}$ is in good agreement with experimental data [45] and, as expected, is found to be systematically lower than the rigid-body value $\mathcal{J}_\perp^{\rm rigid}$ which reads

$$\mathcal{J}_\perp^{\rm rigid} = \frac{2}{5}mR^2\left(1+\sqrt{\frac{5}{16\pi}}\beta\right),$$

for an ellipsoidal shape with axial quadrupole deformation parameter β [66]. In this definition, m is the nucleus mass and $R = 1.2A^{1/3}$ (fm) the nuclear radius. We will therefore use both $\mathcal{J}_\perp^{\rm D1S}$-values and $\mathcal{J}_\perp^{\rm rigid}$-values evaluated for $\beta = \beta_0$ (see subsect. 4.1) to calculate $E_{\rm rot}^{J,K}$ and discuss how these values affect our combinatorial results. It is worth mentioning here that the stronger the pairing field, the lower $\mathcal{J}_\perp^{\rm D1S}$ is.

It is clear that the rotational energy given by eq. (26) modifies the position of the band head states with $K \neq 0$. Indeed, if an intrinsic state K^P is found at an energy E_K in the nucleus intrinsic frame, the corresponding level in the laboratory frame is shifted up by the zero-point rotational energy $K/2\mathcal{J}_\perp$. Therefore, the vibrational energies of table 2 must be shifted down when used in our level density calculations to account for this effect. For the $(\lambda, \mu) = (3, 0)$ mode, the energy is obtained by extrapolating the experimental sequence of $1^-, 3^-$ and 5^- levels.

5 Comparisons with experimental data

This section is devoted to the analysis of the predictions based on our combinatorial approach. We first compare in subsect. 5.1 the results obtained using various assumptions described in sect. 4 with experimental data for excitation energy U of the order of the neutron binding energy B_n. In particular, we study the effect of several treatments of pairing corrections as well as the role played by the vibrational and rotational effects on our predictions. Our goal is to analyze the various approximations of our approach, to see which ones have the strongest influence on the predictions. We then compare in subsect. 5.2 our combinatorial results for $U \ll B_n$ where discrete levels are experimentally observed.

5.1 Average level spacings for $U \approx B_n$

5.1.1 Definitions

The most often used experimental data in level density studies is the density of s-wave neutron resonances. When one considers a reaction between a target of spin J_t and parity π_t and an incident neutron with low energy, one observes resonances in cross-sections which reflect the existence of excited levels in the compound nucleus. For s-wave (*i.e.*, $\ell = 0$) resonances the relationship between the mean spacing D_0 of these resonances and the level density of the compound nucleus is thus

$$D_0 \approx \left[\rho(B_n + W/2, J_t + 1/2, \pi_t) + \rho(B_n + W/2, J_t - 1/2, \pi_t)\right]^{-1} , \quad (27)$$

if $J_t \neq 0$, and

$$D_0 \approx \left[\rho(B_n + W/2, 1/2, \pi_t)\right]^{-1} , \quad (28)$$

otherwise. In these equations, W is the energy width used to determine the experimental D_0-values. It is generally of the order of 1 keV except for closed-shell nuclei or light nuclei where it is rather of the order of several tens of keV [72]. When W is large, derived theoretical D_0-values might be different depending upon whether W is accounted for or not. To check whether this is true or not, we have extracted theoretical D_0-values using the W-values tabulated in [72] and compared them with theoretical D_0-values obtained assuming $W = 0$. It appears that accounting or not for W yields differences for the theoretical D_0-values which are of the order of the size of the points in figs. 3-5.

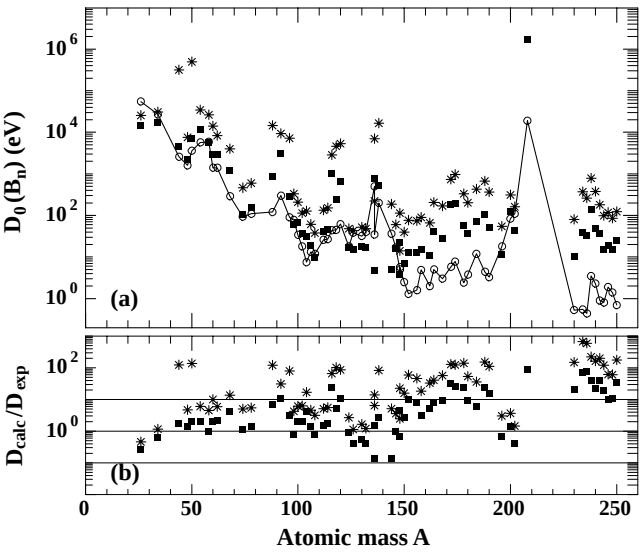

Fig. 3. (a) Mean spacing D_0 of the s-wave neutrons resonances at B_n as a function of the atomic mass. The circles represent the experimental D_0-values of ref. [66] (the line is only used to guide the eye). (b) Ratio between calculated and experimental D_0-values. In both panels, the full squares (respectively the stars) represent the results obtained with (respectively without) inclusion of the quadrupole and octupole phonons.

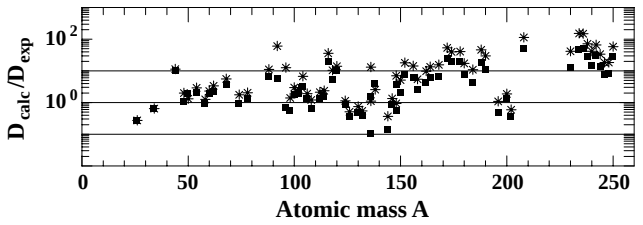

Fig. 4. Ratio between calculated and experimental D_0-values. The full squares (respectively the stars) represent the results obtained with the microscopic HFB + D1S pairing correction and three (respectively one) coupled phonons.

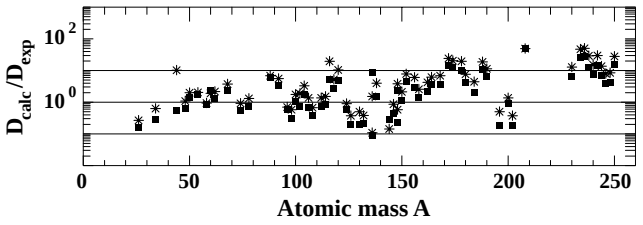

Fig. 5. Ratio between calculated and experimental D_0-values. The full squares (respectively the stars) represent the results obtained with a decreasing (respectively constant) microscopic HFB + D1S pairing correction when the excitation energy increases (see subsect. 3.2 for more details).

Table 3. Nuclei parameters. J^π is the target spin. B_n in MeV, and D_0 in eV.

Z	N	B_n	J^π	D_0	β_0
12	14	11.09	$5/2^+$	$(55 \pm 17)10^3$	−0.31
16	18	11.42	$3/2^+$	$(27 \pm 10)10^3$	−0.17
20	24	11.13	$7/2^-$	$(2.6 \pm 0.4)10^3$	0.00
22	26	11.63	$5/2^-$	$(1.6 \pm 0.4)10^3$	0.14
22	28	10.94	$7/2^-$	$(3.6 \pm 0.9)10^3$	0.00
24	30	9.72	$3/2^-$	$(5.7 \pm 2.0)10^3$	0.22
26	32	10.05	$1/2^-$	$(5.9 \pm 1.5)10^3$	0.22
28	32	11.39	$3/2^-$	$(1.4 \pm 0.3)10^3$	−0.15
28	34	10.56	$3/2^-$	$(1.4 \pm 0.2)10^3$	−0.20
30	38	10.20	$5/2^-$	290 ± 30	−0.14
32	42	10.20	$9/2^+$	93 ± 10	0.17
34	44	10.50	$1/2^-$	110 ± 20	0.15
38	50	11.11	$9/2^+$	121 ± 13	0.00
40	52	8.64	$5/2^+$	300 ± 80	0.00
42	54	9.15	$5/2^+$	91 ± 11	0.00
42	56	8.64	$5/2^+$	78 ± 10	0.07
44	56	9.67	$5/2^+$	34 ± 7	0.19
44	58	9.22	$5/2^+$	18 ± 2	0.20
44	60	8.90	$3/2^+$	7.5 ± 3.8	0.27
46	60	9.56	$5/2^+$	13.3 ± 1.7	0.20
46	62	9.22	$5/2^+$	12 ± 2	0.21
48	64	9.40	$1/2^+$	26 ± 4	0.17
48	66	9.04	$1/2^+$	27 ± 3.5	0.18
50	66	9.56	$1/2^+$	44 ± 22	0.00
50	68	9.33	$1/2^+$	45 ± 10	0.00
50	70	9.11	$1/2^+$	62 ± 12	0.00
52	72	9.43	$1/2^+$	18 ± 4	0.15
52	74	9.11	$1/2^+$	38 ± 3	0.15
54	76	9.26	$1/2^+$	32 ± 3	0.11
54	78	8.94	$3/2^+$	40 ± 15	0.11
54	82	8.06	$3/2^+$	500 ± 100	0.00
56	80	9.11	$3/2^+$	35 ± 9	0.00
56	82	8.61	$3/2^+$	200 ± 65	0.00
60	84	7.82	$7/2^-$	36.5 ± 4	0.00
60	86	7.57	$7/2^-$	17 ± 1.6	0.16
60	88	7.33	$5/2^-$	5 ± 2	0.21
62	86	8.14	$7/2^-$	5.7 ± 0.5	0.16
62	88	7.99	$7/2^-$	2.5 ± 0.25	0.21
62	90	8.26	$5/2^-$	1.3 ± 0.2	0.32
64	92	8.54	$3/2^-$	1.6 ± 0.16	0.33
64	94	7.94	$3/2^-$	4.9 ± 0.4	0.34
66	96	8.20	$5/2^+$	2 ± 1.2	0.35
66	98	7.66	$5/2^-$	5 ± 0.8	0.35
68	100	7.77	$7/2^+$	3 ± 0.5	0.35
70	102	8.02	$1/2^-$	5.8 ± 0.5	0.34
70	104	7.47	$5/2^-$	7.8 ± 0.9	0.34
72	106	7.63	$7/2^-$	2.4 ± 0.3	0.30
72	108	7.39	$9/2^+$	3.8 ± 0.38	0.29
74	110	7.41	$1/2^-$	12 ± 1	0.25
76	112	7.99	$1/2^-$	4.4 ± 0.2	0.22
76	114	7.79	$3/2^-$	3.3 ± 0.2	0.19
78	118	7.92	$1/2^-$	18 ± 3	0.13
80	120	8.03	$1/2^-$	84 ± 18	−0.10
80	122	7.75	$3/2^-$	110 ± 20	−0.07
82	126	7.37	$1/2^-$	$(19 \pm 6)10^3$	0.00
90	140	6.79	$5/2^+$	0.53 ± 0.15	0.25
92	142	6.84	$5/2^+$	0.55 ± 0.05	0.27
92	144	6.55	$7/2^-$	0.44 ± 0.06	0.28
92	146	6.15	$1/2^+$	3.5 ± 0.8	0.28
94	146	6.53	$1/2^+$	2.3 ± 0.1	0.29
94	148	6.31	$5/2^+$	0.9 ± 0.1	0.29
96	148	6.80	$5/2^+$	0.81 ± 0.1	0.30
96	150	6.46	$7/2^+$	1.9 ± 0.8	0.29
96	152	6.21	$9/2^-$	1.4 ± 0.3	0.29
98	152	6.63	$9/2^-$	0.7 ± 0.1	0.30

Since we only deal here with even-even compound nuclei, we use eq. (27) to compare the experimental D_0-values with those deduced from our combinatorial approach. At the present stage, our predictions only depend on the arbitrary energy unit ε_0 (see eq. (14)) used in the discretization of the excitation energies. It is clear that the higher ε_0, the less accurate our calculations are. Moreover, ε_0 must be of the order of the width W appearing in eqs. (27) and (28). We have therefore adopted the value $\varepsilon_0 = 10$ keV, as mentioned previously in subsubsect. 2.1.4.

We show in table 3 the list of Z and N-values relevant to the even-even compound nuclei considered in our study, the experimental D_0-values taken from ref. [66], as well as the axial deformation parameter β_0 obtained from our HFB + D1S microscopic mean-field calculations. Of course, other tabulations of experimental D_0-values can be found in the literature with, sometimes quite important differences, especially for light or nearly magic nuclei. For example, differences within a factor 2-3 exist for such nuclei between the compilations in refs. [66] and [72]. However, changing the set of experimental data does not significantly modify the overall comparisons that follow in figs. 3-5, since such important differences only concern a very small number of nuclei among the 65 nuclei considered in the present study.

5.1.2 Quadrupole and octupole isoscalar vibrations

We first study the specific role played by the vibrational states. For this purpose, we compare in fig. 3 the results obtained by shifting the microscopic intrinsic state densities with the constant HFB + D1S pairing energy with and without inclusion of both quadrupole and octupole vibrational states. The number of coupled phonons considered in this case is equal to two, and the microscopic moments of inertia $\mathcal{J}_\perp^{\mathrm{D1S}}$ are used to construct the rotational bands for deformed nuclei.

As can be seen, ignoring the vibrational states leads to an overall overestimate of the experimental D_0-values. The only exception is for the mass regions $120 < A < 144$ and $A \approx 200$, where the experimental data are quite well reproduced. For ^{208}Pb, the calculation of $D_0(B_n)$ is even impossible when vibrational states are ignored since no levels with correct spin and parity (*i.e.*, 0^- and 1^-) are here predicted below 8.5 MeV. Including the vibrational states clearly improves the overall agreement be-

tween experimental and theoretical D_0-values, even if the global overestimate persists. Of course, for the mass regions where a good agreement was obtained without considering the vibrational states, the level density is now too high. This discrepancy may be due to the assumed axial symmetry which is known to be broken for nuclei close to sphericity such as ^{124,126}Te, ^{130,132}Xe, ^{136}Ba, ^{144}Nd as well as ^{196}Pt and ^{200,202}Hg. In fact, these nuclei are rather soft against triaxial deformation and it is thus not surprising that our model predictions break down. However, further work is needed to treat such nuclei and verify the latter statement.

In order to measure the quality of the predictions, we use the mean square deviation factor f defined as

$$f = \exp\left[\frac{1}{N_{\rm exp}}\sum_{i=1}^{N_{\rm exp}}\left(\ln\frac{D^i_{\rm calc}}{D^i_{\rm exp}}\right)^2\right]^{1/2}, \qquad (29)$$

where $D^i_{\rm calc}$ (respectively $D^i_{\rm exp}$) is the calculated (respectively experimental) $\ell = 0$ mean resonances spacing for the i-th nucleus, and $N_{\rm exp}$ is the total number of nuclei under consideration. We then get $f = 7.25$, when vibrational states are included, to be compared with $f = 32.62$ obtained without including vibrational states.

Finally, one can observe overestimates in the rare-earth and actinide mass regions, as well as for spherical nuclei (for $A \approx 90, 120, 140, 208$). In the latter case, multiphonons vibrational states with $N \geq 3$ are believed to occur because of the spherical symmetry. Therefore, we have increased the number of coupled phonons in the calculations to see how this affects our predictions.

5.1.3 Multiphonons

As mentioned in subsect. 2.2, the number of phonons which may be coupled is limited for physical reasons. Experimentally, two-phonon states are well established [52–63], and possible three-phonon states have also been considered [73,74]. We therefore study in fig. 4 the influence of a variation in the number of coupled phonons on our predictions.

As can be seen, the larger the number of coupled phonons, the better the overall agreement between theoretical predictions and the experimental data is. For 1, 2 and 3 coupled phonons, the deviation factor (29) is 11.25, 7.24 and 6.27, respectively. One can however still notice a persistent and significant disagreement in the rare-earth and actinide mass regions as well as for spherical nuclei. Concerning the nuclei for which the level density was previously overestimated, the increase in the number of coupled phonons has of course not improved the agreement between theoretical and experimental D_0-values, but the differences obtained when considering two (see fig. 3) or three coupled phonons (see fig. 4) are not significant. Therefore, the number of coupled phonons is probably not the most crucial point to improve our predictions. In fact, according to Soloviev [75], such overestimates might be explained by the fact that vibrational modes with multipolarity λ different from 2 and 3 have not been accounted for in our approach. For instance, for spherical nuclei, one could try to include $\lambda = 5$ vibrational states. In the rare-earth and actinide mass regions, magnetic dipole modes which have been observed for excitation energies between 2 and 3 MeV [76–84], could also have an influence on our predictions.

5.1.4 Dipole and hexadecapole vibrational modes

In order to evaluate the effect of missing vibrational states with multipolarity different from 2 or 3, we have included in the rare-earth and actinide regions the magnetic dipole (usually known as scissor) mode which has been well studied [76–84] since its discovery in 1984 [85]. The improvement obtained is typically of the order of 10 percent (the deviation factor now becomes $f = 6.11$ instead of 6.27). This result is not significant enough to be appreciated on a plot. The weak effect of these states could be a consequence of their relatively high excitation energy when compared to that for quadrupole and octupole vibrations. We therefore believe that inclusion of other multipole states, such as hexadecapole states, could have a more significant effect on our predictions. Indeed, in the mass regions $A \approx 170$, for instance, hexadecapole states have been observed with low excitation energy (of the order of 1.5 MeV) [86–89], and could thus have a stronger influence than the magnetic dipole modes. The same remark holds true for closed-shell nuclei [90] where the strong overestimate of our predictions observed in figs. 3, and 4 could also be reduced in the same way.

We have tried to account for such states assuming all hexadecapole modes located at 2 MeV, for the actinides of table 2. As expected, the level densities increase and consequently the theoretical D_0-values get closer to the experimental values. On the average, theoretical values are reduced by almost a factor 2, which is however not enough to obtain a perfect agreement with experimental data. It is therefore necessary to study the other key ingredients of our approach, that is to say, the rotational band construction and the pairing treatment that we have used before concluding whether including more vibrational states is the key ingredient to obtain a better agreement with experimental data.

5.1.5 Rigid versus superfluid moments of inertia

Until now, we have used microscopic moments of inertia deduced from HFB + D1S calculations. It is however well known that the moment of inertia increases with excitation energy as the consequence of gradual weakening of pairing correlations. We have thus performed the same D_0 calculations as in the previous paragraph, this time with the rigid-body values $\mathcal{J}_\perp^{\rm rigid}$ for the moments of inertia used to build rotational bands. This rigid-body value is about 2 or 3 times bigger than $\mathcal{J}_\perp^{\rm D1S}$. However, the results in this case are not very different from those obtained using $\mathcal{J}_\perp^{\rm D1S}$. Indeed, the calculated mean spacings using

$\mathcal{J}_\perp^{\rm rigid}$ are only about 1 percent lower than those predicted when $\mathcal{J}_\perp^{\rm D1S}$ is employed. It is therefore clear that the value of the moment of inertia is not of key importance to improve significantly the agreement between experimental and theoretical D_0-values at B_n.

5.1.6 Energy-dependent pairing correction

We now study the results obtained using the method described in subsect. 3.2 to account for the decrease of the pairing shift when the excitation energy increases. The results obtained are plotted in fig. 5 and compared with those obtained with the constant HFB + D1S shift (see fig. 1). In this figure, three coupled phonons are considered.

As can be seen, a little improvement is obtained but the overestimate in the rare-earth and actinide mass regions persists. The observed improvement is stemming from the fact $\Delta_{\rm HFB}^{\rm combi}$ is always weaker than the constant HFB + D1S shift of fig. 1 and, consequently, the level densities (respectively D_0-values) calculated using $\Delta_{\rm HFB}^{\rm combi}$ are stronger (respectively weaker) than when the constant HFB + D1S shift is employed. The improvement is particularly significant for $A \approx 120$, the mass region which corresponds to the three spherical nuclei ^{116,118,120}Sn. The deviation factor is now $f = 4.55$. Therefore, using the energy-dependent pairing correction $\Delta_{\rm HFB}^{\rm combi}$ introduced in subsect. 3.2 appears to play a more important role than coupling three instead of two phonons.

To further investigate the quality as well as the behavior of our combinatorial energy-dependent pairing correction $\Delta_{\rm HFB}^{\rm combi}$, we compare it, in fig. 6, with the widely employed analytical approximation [91] of the energy-dependent pairing correction $\Delta_{\rm SM}$ of the superfluid model approach [26,27], and with $\Delta_{\rm HFB}^{\rm temp}$ obtained from temperature dependent HFB + D1S calculations for ^{230}Th. The choice of ^{230}Th is simply due to the fact that for such a heavy nucleus, the single-particle states density around the Fermi level is high, so that the shell structures are less important for low excitation energies.

The $\Delta_{\rm HFB}^{\rm temp}$-values are obtained, for a given temperature, with the help of eqs. (23) and (24) for protons (fig. 6(b)) and neutrons configurations (fig. 6(c)), respectively, and by summing these values for proton-neutron configurations (fig. 6(a)). The excitation energy corresponding to a given temperature is simply given by the difference between the nucleus binding energy corresponding to that temperature and the binding energy obtained for a zero temperature. Concerning the $\Delta_{\rm SM}$-values, they are obtained using the method described in ref. [91] with a level density parameter given by the Ignatyuk *et al.* formula [33] and are only plotted here to guide the eye with the widely used model of ref. [91]. These values should certainly not be considered as absolute references ensuring the reliability of the microscopic $\Delta_{\rm HFB}^{\rm temp}$-values. On the contrary, the parameters required to calculate the $\Delta_{\rm SM}$-values have been taken such that the analytic approximation reproduces roughly the behavior of $\Delta_{\rm HFB}^{\rm temp}$-values,

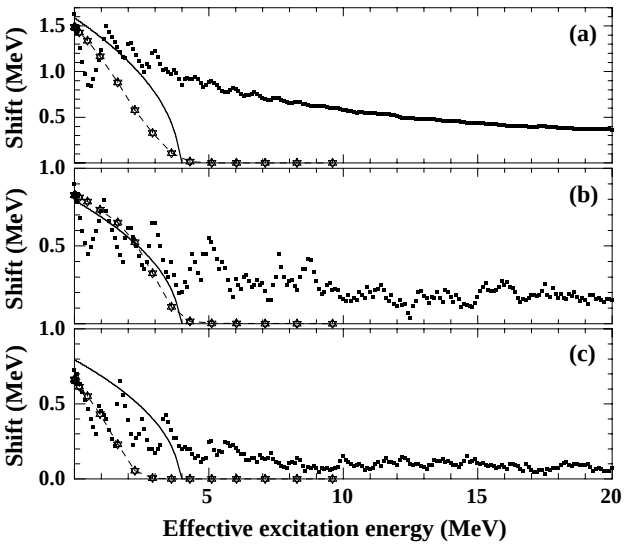

Fig. 6. Comparison between our pairing shift $\Delta_{\rm HFB}^{\rm combi}$ (full squares), the energy-dependent pairing correction obtained in the superfluid model approach $\Delta_{\rm SM}$ (full line) and temperature-dependent pairing energy $\Delta_{\rm HFB}^{\rm temp}$ (dashed lines with stars) for ^{230}Th. The three panels (a), (b) and (c) correspond to the shift applied to proton-neutron, proton and neutron configurations, respectively.

which suggests that the approximation of ref. [91] is appropriate to describe reasonably well a more realistic theoretical (but much more time consuming) approach.

It is interesting to notice in fig. 6 that, whereas the analytic approximation to the superfluid model [91] does not distinguish between proton and neutron $\Delta_{\rm SM}$-values, our approach, as well as the temperature-dependent approach does. Moreover, apart from the low-energy oscillations of $\Delta_{\rm HFB}^{\rm combi}$ due to the discrete nature of the one-particle–one-hole excitations, $\Delta_{\rm HFB}^{\rm combi}$ and $\Delta_{\rm HFB}^{\rm temp}$ display rather similar behaviors for low excitation energies. However, both $\Delta_{\rm HFB}^{\rm temp}$ and $\Delta_{\rm SM}$ vanish above a given critical energy $U_{\rm crit}$ (which is here of the order of 4 MeV) while $\Delta_{\rm HFB}^{\rm combi}$ does not. The reason is that, in our approach, the Δ_i^k-values used to determine $\Delta_{\rm HFB}^{\rm combi}$ (see subsect. 3.2) are calculated for a zero temperature, and therefore never vanish even if they become negligible with respect to the ε_i^k-values (which explains the observed decrease of $\Delta_{\rm HFB}^{\rm combi}$). In other words, the decrease of the pairing energy $\Delta_{\rm HFB}^{\rm temp}$ as a function of excitation energy is well reproduced by our zero-temperature approximation for excitation energies below 2 or 3 MeV, but the shift we apply, using $\Delta_{\rm HFB}^{\rm combi}$, to particle-hole states with excitation energy higher than $U_{\rm crit}$ is too strong. It is therefore clear that using $\Delta_{\rm HFB}^{\rm temp}$ instead of $\Delta_{\rm HFB}^{\rm combi}$ will enhance the improvement already obtained by introducing $\Delta_{\rm HFB}^{\rm combi}$ instead of a constant pairing shift.

Consequently, we are planning to use $\Delta_{\rm HFB}^{\rm temp}$ instead of $\Delta_{\rm HFB}^{\rm combi}$ in our combinatorial approach to see how the theoretical D_0-values would compare with experimental data. However, such an extension would require time consuming calculations, and would go beyond the scope of the present work.

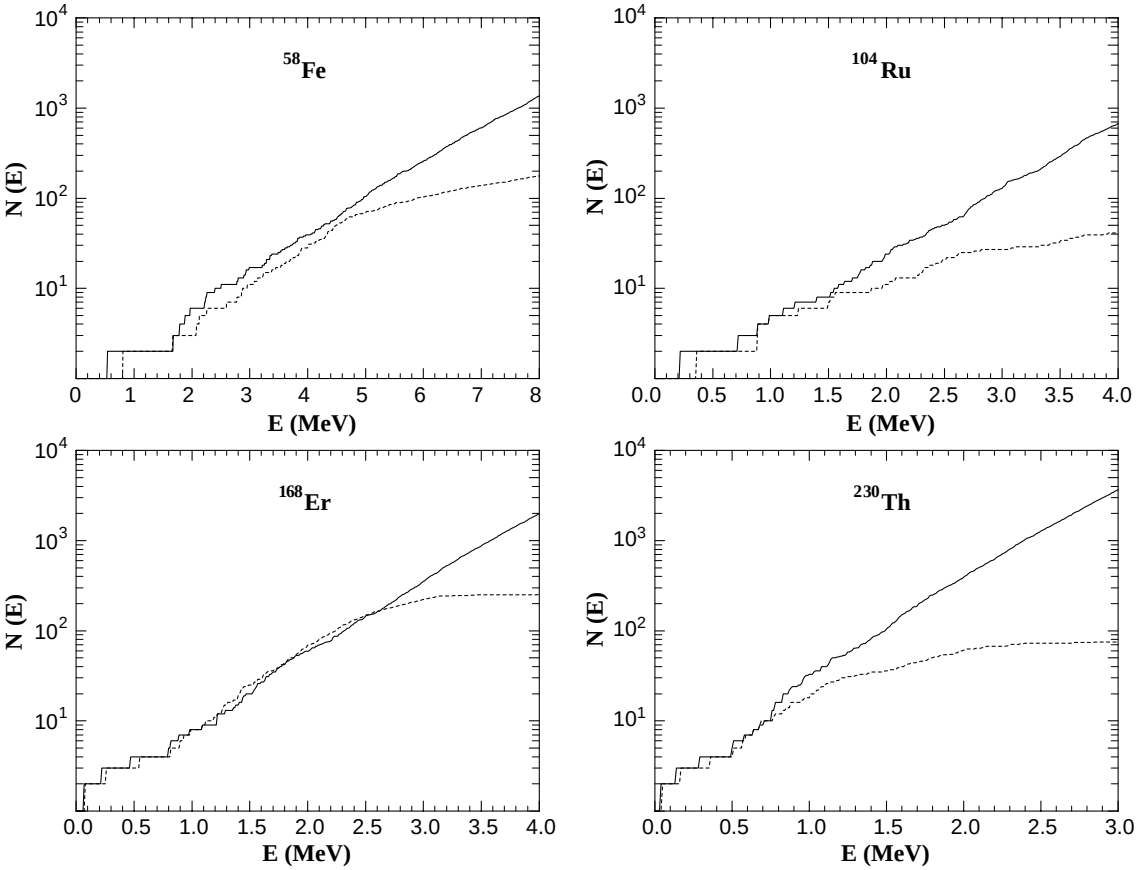

Fig. 7. Comparison between experimental and calculated histograms of cumulated discrete levels when $\mathcal{J}_{\perp}^{\mathrm{D1S}}$ is used to build the rotational bands. The dashed lines represent the experimental data and the full lines our predictions.

5.2 Cumulated discrete levels at low energy

Since we have seen that the pairing correction that we use is good enough to describe the low-energy pairing effects on level densities, we now compare the results obtained with our combinatorial approach for low excitation energies when discrete levels are experimentally observed. For this purpose, we plot in figs. 7 and 8 histograms for both experimental and theoretical cumulated discrete levels of ^{58}Fe, ^{104}Ru, ^{168}Er, and ^{230}Th.

In fig. 7, the theoretical histograms (full lines) have been obtained using the microscopic moment of inertia $\mathcal{J}_{\perp}^{\mathrm{D1S}}$, whereas in fig. 8, $\mathcal{J}_{\perp}^{\mathrm{rigid}}$ has been adopted to build the rotational bands. Also, in both figures three phonons have been coupled and the energy-dependent microscopic pairing correction (see subsect. 3.2) has been used. It is clear that the number of coupled phonons is not of key importance in these figures, since we study a very low excitation energy region where only one coupled phonon must be considered. As can be seen, the combinatorial approach reproduces quite well the experimental data (dashed lines). Furthermore, comparing fig. 7 and fig. 8, one can notice that using $\mathcal{J}_{\perp}^{\mathrm{D1S}}$ leads to better agreements than with $\mathcal{J}_{\perp}^{\mathrm{rigid}}$ at low energy. However, it is interesting to notice that for ^{168}Er, for which the levels spectroscopy is expected to be almost complete up to 2.5 MeV, our predictions underestimate the experimental data above 1 MeV when $\mathcal{J}_{\perp}^{\mathrm{D1S}}$ is used, while the experimental data are overestimated if $\mathcal{J}_{\perp}^{\mathrm{rigid}}$ is employed. This observation suggests that the agreement between predictions and experimental data might be improved by accounting for the energy dependence of the moment of inertia, but further comparisons are required to draw a definite conclusion on this issue.

Above a few MeV of excitation energy, the experimental resolution is not good enough to identify all the discrete levels, which results in a saturation of the experimental histogram. This is why there is a strong disagreement above a few MeV between our results and the experimental data.

6 Conclusions

An accurate combinatorial approach permitting calculations of both particle-hole and total level densities as functions of energy, spin and parity has been presented. This method, which relies upon the adiabatic approximation, has been implemented using the single-particle spectra provided by Hartree-Fock-Bogoliubov microscopic calculations based on the D1S Gogny effective interaction performed for 65 even-even nuclei. It has been shown that it

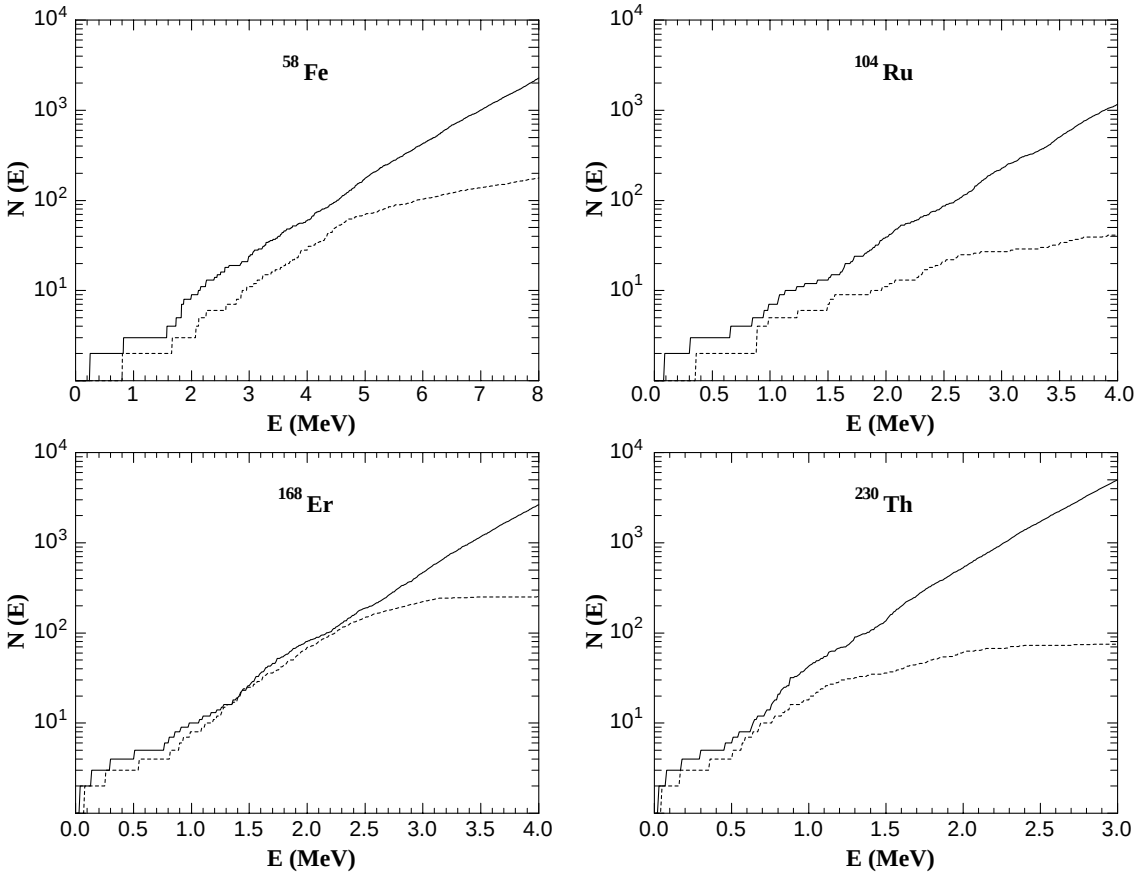

Fig. 8. Comparison between experimental and calculated histograms of cumulated discrete levels when $\mathcal{J}_{\perp}^{\mathrm{rigid}}$ is used to build the rotational bands. The dashed lines represent the experimental data and the full lines our predictions.

is possible to reproduce reasonably well the experimental data on level densities for excitation energies close to the neutron binding energy, provided that the vibrational and rotational enhancements were accounted for. At low excitation energy, this method has also proved its power to reproduce rather well the cumulated discrete level histograms. Such a predictive power should be very interesting to determine low-energy level density laws —which play a crucial role in compound nucleus cross-section calculations— when no experimental information is available, especially for nuclei far from the valley of stability. For such nuclei, the required vibrational-mode energies would be predicted from solving a collective Hamiltonian built from HFB + D1S calculations, as explained in ref. [45].

However, some discrepancies remain between measurements and predictions for excitation energies close to the neutron binding energy. Indeed, a systematic overestimate of the mean spacing of s-wave neutron resonances is observed for the rare-earth and actinide mass regions. Several explanations are possible:

i) First, a better knowledge of the octupole mode energies as well as inclusion of hexadecapole vibrational modes (or/and modes with higher multipolarities) will certainly improve the agreement of our predictions with experimental data.

ii) Second, accounting for the so-called particle-vibration coupling may also significantly modify the results. It is indeed known that when vibrational states are accounted for in self-consistent microscopic methods, the gap between the last occupied and the first empty state is reduced and the level density is consequently increased. The higher the gap, the more this reduction is important. This is probably the reason why the disagreement between experimental data and our combinatorial results is so important for ^{208}Pb as well as for the $A \approx 90$ and $A \approx 120$ mass regions where important gaps are known to occur.

iii) Finally, as mentioned in subsubsect. 5.1.6, the treatment of pairing correlations that we have considered has to be improved, to account for the known vanishing of pairing effects above a critical excitation energy [26, 27]. Indeed, it has been shown that energy-dependent pairing shift improve significantly the quality of our predictions, and the agreement will certainly be better if the vanishing of pairing effect is more correctly accounted for. We believe that such an improvement is of crucial importance before studying deeper the two aforementioned effects. We hope to report on this issue in the near future.

Another issue is the energy dependence of the moment of inertia used to build the rotational bands in de-

formed nuclei [92,93]. If the moments of inertia yielded by HFB + D1S microscopic calculations are rather realistic for the first discrete levels, it is also known that they are too weak when the excitation energy increases and should also be modified because of the energy dependence of the nucleus deformation. However, this point is difficult to study for excitation energies close to the neutron binding energy since the modification of the s-wave neutron resonances mean spacings is only of the order of 1 percent when the rigid-body values are used instead of the superfluid ones. Such an effect could only be studied with experimental data covering a wide enough excitation energy range.

Last, but not least, it is important to remember that all our combinatorial results rely on the single-particle levels properties obtained from Hartree-Fock-Bogoliubov calculations based on the D1S Gogny force. Therefore, it would be interesting to perform similar studies using other effective forces.

Our method has not yet been applied to odd or odd-odd nuclei. It is thus a challenge to see if the overall agreement here obtained for even-even nuclei could also be obtained for odd and odd-odd nuclei. It would be also useful to compare our microscopic approach with usually employed analytical formulae. Indeed, these analytical formulae are fitted on scarce data which moreover never extend beyond 10 MeV or so. Since our combinatorial approach has proved its predictive power, we are planning to use our results to study the energy behaviors of the level density parameter and of the parity distribution for instance. In fact, the comparison of our results with those from the extensively employed Ignatyuk *et al.* formula is presently underway.

The authors are grateful to J.F. Berger for continuous encouragements and stimulating discussions.

References

1. H.A. Bethe, Rev. Mod. Phys. **9**, 69 (1937).
2. T. Ericson, Adv. Phys. **9**, 425 (1960).
3. F.C. Williams, Nucl. Phys. A **166**, 231 (1971).
4. E. Běták, J. Dobeš, Z. Phys. A **279**, 319 (1976).
5. P. Obložinský, Nucl. Phys. A **453**, 127 (1986).
6. A. Anzaldo-Meneses, Z. Phys. A **353**, 295 (1995).
7. S. Hilaire, J.P. Delaroche, A.J. Koning, Nucl. Phys. A **632**, 417 (1998).
8. C. Kalbach, J. Phys. G: Nucl. Part. Phys. **21**, 1499 (1995).
9. A.V. Ignatyuk, Yu.V. Sokolov, Sov. J. Nucl. Phys. **17**, 376 (1973).
10. C.Y. Fu, Nucl. Sci. Eng. **92**, 440 (1986); **86**, 344 (1984).
11. J.F. Berger, M. Martinot, Nucl. Phys. A **226**, 391 (1974).
12. M. Herman, G. Reffo, Phys. Rev. C **36**, 1546 (1987).
13. A.H. Blin *et al.*, Nucl. Phys. A **456**, 109 (1986) and references therein.
14. F. Garcia *et al.*, Phys. Rev. C **60**, 064311 (1999).
15. D.J. Dean, S.E. Koonin, Phys. Rev. C **60**, 054306 (1999).
16. F.C. Williams *et al.*, Nucl. Phys. A **187**, 225 (1972).
17. M. Hillman, J.R. Grover, Phys. Rev. **185**, 1303 (1969).
18. N. Cerf, Phys. Rev. C **50**, 836 (1994).
19. Y. Alhassid *et al.*, Phys. Rev. Lett. **83**, 4265 (1999).
20. W.E. Ormand, Phys. Rev. C **56**, R1678 (1997).
21. J.A. White *et al.*, Phys. Rev. C **61**, 034303 (2000).
22. B. Strohmaier *et al.*, Phys. Rev. C **36**, 1604 (1987).
23. S.M. Grimes, T.N. Massey, Phys. Rev. C **51**, 606 (1995).
24. B.K. Agrawal, A. Ansari, Nucl. Phys. A **640**, 362 (1998) and references therein.
25. S. Goriely, Nucl. Phys. A **605**, 28 (1996).
26. M. Sano, S. Yamasaki, Prog. Theor. Phys. **29**, 397 (1963).
27. P. Decowski *et al.*, Nucl. Phys. A **110**, 129 (1968).
28. F.N. Choudhury, S. Das Gupta, Phys. Rev. C **16**, 757 (1977).
29. A. Gilbert, A.G.W. Cameron, Can. J. Phys. **43**, 1446 (1965).
30. W. Dilg *et al.*, Nucl. Phys. A **217**, 269 (1973).
31. H. Baba, Nucl. Phys. A **159**, 625 (1970).
32. S.K. Kataria *et al.*, Nucl. Phys. A **349**, 10 (1980)
33. A.V. Ignatyuk *et al.*, Sov. J. Nucl. Phys. **21**, 255 (1975).
34. G. Hansen, A.S. Jensen, Nucl. Phys. A **406**, 236 (1983).
35. T. Døssing, A.S. Jensen, Nucl. Phys. A **222**, 493 (1974).
36. D. Gogny, in *Proceedings of the International Conference on Nuclear Physics, Munich, 1973,* edited by J. De Boer, H.J. Mang (North Holland, Amsterdam, 1973); in *Proceedings of the International Conference on Nuclear Self-consistent Fields, Trieste, 1975,* edited by G. Ripka, M. Porneuf (North Holland, Amsterdam, 1973).
37. J. Dechargé, D. Gogny, Phys. Rev. C **21**, 1568 (1980).
38. J.F. Berger, M. Girod, D. Gogny, Comput. Phys. Commun. **63**, 365 (1991).
39. M. Girod, B. Grammaticos, Phys. Rev. C **27**, 2317 (1983).
40. J.F. Berger, M. Girod, D. Gogny, Nucl. Phys. A **428**, 23c (1984).
41. R.K. J. Sandor *et al.*, Phys. Rev. C **43**, R2040 (1991).
42. M. Girod *et al.*, Phys. Rev. Lett. **62**, 2452 (1989).
43. M. Girod *et al.*, Phys. Rev. C **45**, R1420 (1992).
44. M. Girod *et al.*, Phys. Lett. B **325**, 1 (1994).
45. J. Libert, M. Girod, J.P. Delaroche, Phys. Rev. C **60**, 054301 (1999).
46. S. Péru, M. Girod, J.F. Berger, Eur. Phys. J. A **9**, 35 (2000).
47. M. Girod *et al.*, Phys. Rev. C **37**, 2600 (1988).
48. X.H. Phan *et al.*, Phys. Rev. C **38**, 1173 (1988); **39**, 1645(E) (1989).
49. W. Boeglin *et al.*, Nucl. Phys. A **477**, 399 (1988).
50. J.P. Delaroche *et al.*, Phys. Rev. C **50**, 2332 (1994).
51. A. Bohr, Mat.-Fys. Medd. K. Dan. Vidensk. Selsk. **26**, 14 (1952).
52. M.R. Schmorak *et al.*, Phys. Rev. Lett. **24**, 1507 (1970).
53. G. Coleman, R.A. Meyer, Phys. Rev. C **13**, 847 (1976).
54. S. Lunardi *et al.*, Phys. Rev. Lett. **53**, 1531 (1984).
55. R.A. Gatenby *et al.*, Phys. Rev. C **41**, R414 (1990).
56. H.J. Wollersheim *et al.*, Z. Phys. A **341**, 137 (1992).
57. T. Belgya *et al.*, Phys. Rev. C **52**, R2314 (1995).
58. L. Bargioni *et al.*, Phys. Rev. C **51**, R1057 (1995).
59. M. Wilhelm *et al.*, Phys. Rev. C **54**, R449 (1996).
60. C. Fahlander *et al.*, Phys. Lett. B **388**, 475 (1996).
61. P.E. Garrett *et al.*, Phys. Rev. Lett. **78**, 4545 (1997).
62. R. Schwengner *et al.*, Nucl. Phys. A **620**, 277 (1997).
63. M. Wilhelm *et al.*, Phys. Rev. C **57**, 577 (1998).
64. V.G. Soloviev, Nucl. Phys. A **633**, 247 (1998).

65. A. Bohr, B.R. Mottelson, *Nuclear Structure* (W.A. Benjamin, New York, 1975) p. 7.
66. A.S. Iljinov *et al.*, Nucl. Phys. A **543**, 517 (1992).
67. R.B. Firestone, *Tables of Isotopes*, edited by V.S. Shirley (John Wiley & Sons, New York, 1996).
68. P.D. Cottle, N.V. Zamfir, Phys. Rev. C **54**, 176 (1996).
69. P.C. Sood, At. Data Nucl. Data Tables **47**, 89 (1991).
70. D.R. Inglis, Phys. Rev. **103**, 1786 (1956).
71. S.T. Belyaev, Nucl. Phys. **24**, 322 (1961).
72. Reference Input Parameter Library (RIPL), `http://iaeand.iaea.or.at/ripl/resonances.htm`, Average Neutron Resonance Parameters and Other Data collected in Beijing.
73. R. Georgii *et al.*, Phys. Lett. B **351**, 82 (1995).
74. R. Georgii *et al.*, Nucl. Phys. A **592**, 307 (1995).
75. V.G. Soloviev, L.A. Malov, Nucl. Phys. A **196**, 433 (1972).
76. C. Fransen *et al.*, Phys. Rev. C **57**, 129 (1988).
77. R.D. Herzberg *et al.*, Nucl. Phys. A **563**, 445 (1993).
78. R. Nojarov *et al.*, Nucl. Phys. A **563**, 349 (1993).
79. H. Maser *et al.*, Phys. Rev. C **53**, 2749 (1996).
80. P. Von Brentano *et al.*, Phys. Rev. Lett. **76**, 2029 (1996).
81. P. Sarriguren *et al.*, Phys. Rev. C **54**, 690 (1996).
82. N. Pietralla *et al.*, Nucl. Phys. A **618**, 141 (1997).
83. N. Pietralla *et al.*, Phys. Rev. C **58**, 184 (1998).
84. J. Enders *et al.*, Phys. Rev. C **59**, R1851 (1999).
85. D. Bohle *et al.*, Phys. Lett. B **137**, 27 (1984).
86. R.D. Bagnell *et al.*, Phys. Lett. B **66**, 129 (1977).
87. D.G. Burke *et al.*, Phys. Lett. B **78**, 48 (1978).
88. P.M. Walker *et al.*, Phys. Lett. B **116**, 393 (1982).
89. V.O. Nesterenko *et al.*, Sov. J. Nucl. Phys. **44**, 938 (1986).
90. P.C. Sood *et al.*, Phys. Rev. C **51**, 2798 (1995).
91. A.V. Ignatyuk, Yu.N. Shubin, Izv. AN SSSR, Ser. Fiz. **37**, 1947 (1973).
92. G.D. Dracoulis, Phys. Scri. T **88**, 54 (2000).
93. M. Farine, P. Schuck, X. Viñas, Phys. Rev. A **62**, 013608 (2000).